Ultrafast and Doppler-free femtosecond optical ranging based on dispersive frequency-modulated interferometry

Haiyun Xia,* Chunxi Zhang

School of Instrument Science and Optoelectronics Engineering,
Beijing University of Aeronautics and Astronautics, Beijing 100083, China
**haiyunxia@hotmail.com*

Abstract: An ultrafast and Doppler-free optical ranging system based on dispersive frequency-modulated interferometry is demonstrated. The principle is similar to the conventional frequency-modulated continuous-wave interferometry where the range information is derived from the beat frequency between the object signal and the reference signal. However, a passive and static frequency scanning is performed based on the chromatic dispersion of a transform-limited femtosecond pulse in the time domain. We point out that the unbalanced dispersion introduced in the Mach-Zehnder interferometer can be optimized to eliminate the frequency chirp in the temporal interferograms pertaining to the third order dispersion of the all-fiber system, if the dynamic range being considered is small. Some negative factors, such as the polarization instability of the femtosecond pulse, the power fluctuation of the optical signal and the nonuniform gain spectrum of the erbium-doped fiber amplifier lead to an obvious envelope deformation of the temporal interferograms from the Gaussian shape. Thus a new data processing method is proposed to guarantee the range resolution. In the experiment, the vibration of a speaker is measured. A range resolution of 1.59 μm is achieved with an exposure time of 394 fs at a sampling rate of 48.6 MHz.

OCIS codes: (120.0280) Remote sensing and sensors; (120.3180) Interferometry; (280.3400) Laser range finder; (320.7160) Ultrafast technology; (140.4050) Mode-locked lasers; (140.3510) Lasers, fiber.

References and links

1. J. M. Payne, D. Parker, and R. F. Bradley, "Range finder with fast multiple range capability," Rev. Sci. Instrum. **63**(6), 3311–3316 (1992).
2. R. Dändliker, R. Thalmann, and D. Prongué, "Two-wavelength laser interferometry using superheterodyne detection," Opt. Lett. **13**(5), 339–341 (1988).
3. R. Dandliker, K. Hug, J. Politch, and E. Zimmermann, "High-accuracy distance measurements with multiple-wavelength interferometry," Opt. Eng. **34**(8), 2407 (1995).
4. A. G. Stove, "Linear FMCW radar techniques," Radar and Signal Processing, IEE Proceedings F **139**, 343–350 (1992).
5. E. C. Burrows, and K.-Y. Liou, "High-resolution laser LIDAR utilizing two-section distributed feedback semiconductor laser as a coherent source," Electron. Lett. **26**(9), 577–579 (1990).
6. J. Schwider, and L. Zhou, "Dispersive interferometric profilometer," Opt. Lett. **19**(13), 995–997 (1994).
7. J. Calatroni, A. L. Guerrero, C. Sainz, and R. Escalona, "Spectrally resolved white-light interferometry as a profilometry tool," Opt. Laser Technol. **28**(7), 485–489 (1996).
8. A. Pf Rtner, and J. Schwider, "Dispersion error in white-light linnik interferometers and its implications for evaluation procedures," Appl. Opt. **40**(34), 6223–6228 (2001).
9. D. J. Jones, S. A. Diddams, J. K. Ranka, A. Stentz, R. S. Windeler, J. L. Hall, and S. T. Cundiff, "Carrier-envelope phase control of femtosecond mode-locked lasers and direct optical frequency synthesis," Science **288**(5466), 635–639 (2000).
10. A. Bartels, C. W. Oates, L. Hollberg, and S. A. Diddams, "Stabilization of femtosecond laser frequency combs with subhertz residual linewidths," Opt. Lett. **29**(10), 1081–1083 (2004).
11. J. J. McFerran, W. C. Swann, B. R. Washburn, and N. R. Newbury, "Elimination of pump-induced frequency jitter on fiber-laser frequency combs," Opt. Lett. **31**(13), 1997–1999 (2006).

#115943 - $15.00 USD Received 20 Aug 2009; revised 23 Nov 2009; accepted 29 Nov 2009; published 17 Feb 2010

12. W. C. Swann, J. J. McFerran, I. Coddington, N. R. Newbury, I. Hartl, M. E. Fermann, P. S. Westbrook, J. W. Nicholson, K. S. Feder, C. Langrock, and M. M. Fejer, "Fiber-laser frequency combs with subhertz relative linewidths," Opt. Lett. **31**(20), 3046–3048 (2006).
13. K. Minoshima, and H. Matsumoto, "High-accuracy measurement of 240 m distance in an optical tunnel by using of a compact femtosecond laser," Appl. Opt. **39**(30), 5512–5517 (2000).
14. J. Ye, "Absolute measurement of a long, arbitrary distance to less than an optical fringe," Opt. Lett. **29**(10), 1153–1155 (2004).
15. K.-N. Joo, and S.-W. Kim, "Absolute distance measurement by dispersive interferometry using a femtosecond pulse laser," Opt. Express **14**(13), 5954–5960 (2006), http://www.opticsinfobase.org/abstract.cfm?URI=oe-14-13-5954.
16. W. C. Swann, and N. R. Newbury, "Frequency-resolved coherent lidar using a femtosecond fiber laser," Opt. Lett. **31**(6), 826–828 (2006).
17. H. Xia, and C. Zhang, "Ultrafast ranging lidar based on real-time Fourier transformation," Opt. Lett. **34**(14), 2108–2110 (2009).
18. N. Nishizawa, Y. Chen, P. Hsiung, E. P. Ippen, and J. G. Fujimoto, "Real-time, ultrahigh-resolution, optical coherence tomography with an all-fiber, femtosecond fiber laser continuum at 1.5 microm," Opt. Lett. **29**(24), 2846–2848 (2004).
19. M. Wojtkowski, V. Srinivasan, T. Ko, J. Fujimoto, A. Kowalczyk, and J. Duker, "Ultrahigh-resolution, high-speed, Fourier domain optical coherence tomography and methods for dispersion compensation," Opt. Express **12**(11), 2404–2422 (2004), http://www.opticsinfobase.org/abstract.cfm?URI=oe-12-11-2404.
20. Y. Yasuno, Y. Hong, S. Makita, M. Yamanari, M. Akiba, M. Miura, and T. Yatagai, "In vivo high-contrast imaging of deep posterior eye by 1-um swept source optical coherence tomography and scattering optical coherence angiography," Opt. Express **15**(10), 6121–6139 (2007), http://www.opticsinfobase.org/abstract.cfm?URI=oe-15-10-6121.
21. H. Yoon, and P. Tsiotras, "Spacecraft adaptive attitude and power tracking with variable speed control moment gyroscopes," J. Guid. Control Dyn. **25**(6), 1081–1090 (2002).
22. T. Jannson, "Real-time Fourier transformation in dispersive optical fibers," Opt. Lett. **8**(4), 232–234 (1983).
23. J. Azaña, and M. A. Muriel, "Real-time optical spectrum analysis based on the time-space duality in chirped fiber gratings," IEEE J. Quantum Electron. **36**(5), 517–526 (2000).
24. Y. C. Tong, L. Y. Chan, and H. K. Tsang, "fiber dispersion or pulse spectrum measurement using a sampling oscilloscope," Electron. Lett. **33**(11), 983–985 (1997).
25. F. Hakimi, and H. Hakimi, "Measurement of optical fiber dispersion and dispersion slope using a pair of short optical pulses and Fourier transform property of dispersive medium," Opt. Eng. **40**(6), 1053–1056 (2001).
26. C. Dorrer, "Chromatic dispersion characterization by direct instantaneous frequency measurement," Opt. Lett. **29**(2), 204–206 (2004).
27. R. M. Fortenberry, and W. V. Sorin, "Apparatus for characterizing short optical pulses," U.S. patent 5,684,586 (1997).
28. N. K. Berger, B. Levit, V. Smulakovsky, and B. Fischer, "Complete characterization of optical pulses by real-time spectral interferometry," Appl. Opt. **44**(36), 7862–7866 (2005).
29. T.-J. Ahn, Y. Park, and J. Azaña, "Improved Optical Pulse Characterization Based on Feedback-Controlled Hilbert Transformation Temporal Interferometry," IEEE Photon. Technol. Lett. **20**(7), 475–477 (2008).
30. H. Xia, and J. Yao, "Characterization of Sub-Picosecond Pulses Based on Temporal Interferometry with Real-Time Tracking of Higher-Order Dispersion and Optical Time Delay," J. Lightwave Technol. **27**(22), 5029–5037 (2009).
31. J. Chou, D. R. Solli, and B. Jalali, "Real-time spectroscopy with subgigahertz resolution using amplified dispersive Fourier transformation," Appl. Phys. Lett. **92**(11), 1111021–1111023 (2008).
32. D. R. Solli, J. Chou, and B. Jalali, "Amplified wavelength–time transformation for real-time spectroscopy," Nat. Photonics **2**(1), 48–51 (2008).
33. S. Moon, and D. Y. Kim, "Ultra-high-speed optical coherence tomography with a stretched pulse supercontinuum source," Opt. Express **14**(24), 11575–11584 (2006), http://www.opticsinfobase.org/abstract.cfm?URI=oe-14-24-11575.
34. Y. Park, T.-J. Ahn, J.-C. Kieffer, and J. Azaña, "Optical frequency domain reflectometry based on real-time Fourier transformation," Opt. Express **15**(8), 4597–4616 (2007), http://www.opticsinfobase.org/abstract.cfm?id=131858.
35. R. E. Saperstein, N. Alic, S. Zamek, K. Ikeda, B. Slutsky, and Y. Fainman, "Processing advantages of linear chirped fiber Bragg gratings in the time domain realization of optical frequency-domain reflectometry," Opt. Express **15**(23), 15464–15479 (2007), http://www.opticsinfobase.org/abstract.cfm?uri=oe-15-23-15464.
36. K. Goda, D. R. Solli, and B. Jalali, "Real-time optical reflectometry enabled by amplified dispersive Fourier transformation," Appl. Phys. Lett. **93**(3), 0311061–0311063 (2008).
37. K. Goda, K. K. Tsia, and B. Jalali, "Serial time-encoded amplified imaging for real-time observation of fast dynamic phenomena," Nature **458**(7242), 1145–1149 (2009).
38. G. P. Agrawal, *Nonlinear Fiber Optics*, 3nd ed. San Diego, (CA: Academic, 2001).
39. M. Miyagi, and S. Nishida, "Pulse spreading in a single-mode fiber due to third-order dispersion," Appl. Opt. **18**(5), 678–682 (1979).
40. M. Amemiya, "Pulse broadening due to higher order dispersion and its transmission limit," J. Lightwave Technol. **20**(4), 591–597 (2002).
41. J. Zhang, X. Zhao, X. Hu, and J. Sun, "Sinewave fit algorithm based on total least-squares method with application to ADC effective bits measurement," IEEE Trans. Instrum. Meas. **46**(4), 1026–1030 (1997).

#115943 - $15.00 USD Received 20 Aug 2009; revised 23 Nov 2009; accepted 29 Nov 2009; published 17 Feb 2010

42. J. Capmany, J. Mora, D. Pastor, B. Ortega, and S. Sales, "Microwave Photonic Signal Processing" in *Microwave Photonics: Devices and Applications*, Stavros Iezekiel, ed. (IEEE press, John Wiley, Chichester, 2009) pp.191–237.

1. Introduction

For inherent advantages such as noncontact operation and immunity to electromagnetic interference, optical ranging based on interferometry has drawn extensive attention for scientific and industrial applications. The most notable interferometric techniques for high-resolution optical ranging generally fall into three categories, i.e., the amplitude-modulated interferometry (AMI), the frequency-modulated interferometry (FMI), and the spectrally-resolved interferometry (SRI). In an AMI system [1], the amplitude of the outgoing laser is modulated sinusoidally. Range information is deduced from the phase shift between the object signal and the reference signal. The range should be known beforehand with an accuracy of sub-wavelength to avoid the ambiguity problem. By using modulating frequency of 1.5 GHz, a resolution better than 50 μm over a distance of 120 m was reported [1]. Using heterodyne beatings between two or even more continuous-wave laser sources, the ambiguity problem can be solved [2, 3]. In a FMI system [4], the frequency of the outgoing continuous-wave is modulated linearly and periodically, the object signal and the reference signal are mixed in a photodetector (PD), which yields a beat frequency proportional to the time delay between the two signals. With the chirp rate of the modulation, the range information can be retrieved from the recorded interferograms. A resolution of 0.1μm was demonstrated experimentally [5]. In a SRI system [6], interferograms associated with different spectral components within the broad spectrum of a white-light source are superposed incoherently. After passing through a spectroscope, interferograms are dispersed spacially and then projected onto a CCD camera. The range information can be retrieved from the recorded interferograms. A resolution of 1 nm was reported [7]. One drawback of this technique is that one need equalize the geometrical path lengths in dispersive elements to avoid ghost steps in the measured profile [8].

Recently, with significant developments in the stability, compactness and portability of the femtosecond lasers [9–12], optical ranging based on femtosecond lasers becomes attractive [13–17]. One of the most successful optical ranging based on femtosecond lasers is the optical coherence tomography (OCT) for biomedical imaging. Usually, there is a limited sampling speed for an OCT system. For example, the speed of the optical-path scanner in a cross-correlation-OCT [18], the data transfer rate of a CCD line-scan camera in a SRI-OCT [19] and the speed of the wavelength-scanning source in a FMI-OCT [20] led to sampling speed of 1,900, 16,000 and 28,000 sample/second, respectively.

For some ultrafast dynamic applications, a limited sampling speed may cause a low resolution. For example, magnetic flywheels can combine the energy-storage and the attitude-control functions to increase the payload capacity. To achieve a high torque-output/energy-storage capacity, the spin rate is on the order of 40,000-80,000 revolution per minute (RPM) [21]. To implement a close-loop control, a real-time and noncontact monitoring of the vibration/deformation of the magnetic-bearing-supported flywheel is in great demand. In this paper, a compact and light weight optical ranging system incorporating a passively mode-locked femtosecond fiber laser is demonstrated.

2. Theory

Recently, we demonstrated an ultrafast ranging lidar based on real-time Fourier transformation [17]. The technique is called dispersive frequency-modulation interferometry (DFMI) in this paper, since the active frequency modulation in a conventional continuous-wave FMI is substituted by the dispersion of a femtosecond laser pulse. Effects of the higher-order dispersion associated with the entire system and the unbalanced dispersion introduced in the fiber Mach-Zehnder interferometer (MZI) are analyzed. We prove that DFMI is immune to the Doppler shift associated with the line-of-sight velocity of the target under test.

#115943 - $15.00 USD Received 20 Aug 2009; revised 23 Nov 2009; accepted 29 Nov 2009; published 17 Feb 2010

2.1 system setup

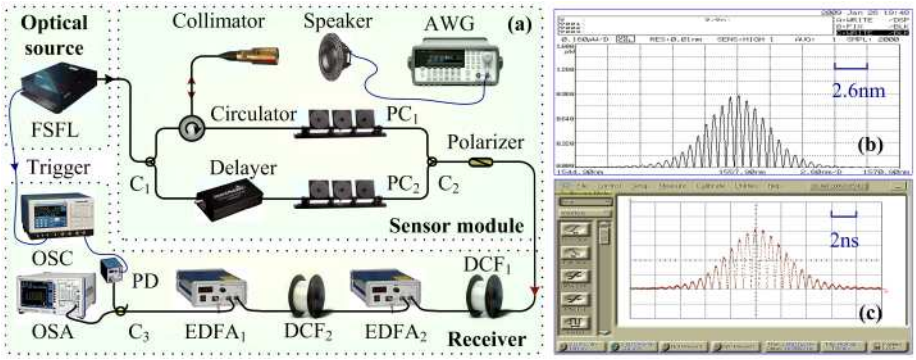

Fig. 1. (a) Schematic of the ultrafast ranging system. FSFL, femtosecond fiber laser; C, fused fiber coupler; AWG, arbitrary waveform generator; PC, polarization controller; DCF, dispersion compensating fiber; EDFA, erbium doped fiber amplifier; PD, photodetector; OSC, oscilloscope; OSA, optical spectrum analyzer. (b) Picture of the spectral interferogram recorded on the OSA (Ando Model AQ6317B). (c) Picture of the temporal interferogram recorded on the OSC (Agilent Model 86116A).

The schematic of the system is shown in Fig. 1(a). The optical source is a passively mode-locked femtosecond fiber laser (IMRA Femtolite 780 Model B-4-FC-PD), which emits a train of pulses with a full width at half maximum (FWHM) of 394 *fs* and a center frequency of 192.31 *THz* at a repetition rate of 48.6 *MHz*. The target under test is a speaker driven by an arbitrary waveform generator (Agilent Model 33250A). The speaker is mounted on a multi-axis tilt stage. The collimator produces a light beam with a divergence of $2\,mrad$ and a beam diameter of $1.5\,mm$. By adjusting the multi-axis tilt stage precisely, one can make sure that the optical axis of the collimator is perpendicular to a tiny reflecting mirror glued on the membrane of the speaker. Thus, the vibration amplitude of the speaker can be incorporated into one arm of the Mach–Zehnder interferometer (MZI) by using an optical fiber circulator. In the other arm of the MZI, an optical time delayer is used to adjust the time delay difference between the reference signal and the object signal. To perform a temporal interference, an in-line polarizer is added at the output end of the MZI. Polarization controllers PC_1 and PC_2 are used to adjust the transmission of the two signals through the polarizer to achieve the largest fringe visibility in the interferogram. In the optical receiver, two coils of dispersion-compensating fiber (DCF) are used in cascade to stretch the femtosecond pulses sufficiently in the time domain. The optical signal is amplified by two erbium-doped fiber amplifiers (EDFA) to guarantee the signal-to-noise ratio in the optical receiver. The temporal interferogram and spectral interferogram are recorded using an oscilloscope (OSC) and an optical spectrum analyzer (OSA), as shown in Fig. 1(b) and Fig. 1(c), respectively.

2.2 Effect of the higher order dispersion on the DFMI

There is a well-known analogy between the paraxial diffraction of a monochromatic beam in space and the temporal dispersion of an ultra-short coherent pulse in an optical dispersive element. Optical elements with high group velocity dispersion, such as dispersive optical fibers [22] and linearly chirped fiber Bragg gratings [23], could be used to implement a real-time dispersive Fourier transformation in the optical domain. There are a lot of successful applications based on this optical-domain signal-processing technique, such as optical fiber dispersion measurement [24–26], complete characterization of ultra-short optical pulses [27–30], real-time spectroscopy [31, 32], and optical frequency-domain reflectometry [33–37].

The real-time dispersive Fourier transformation is implemented under the temporal Fraunhofer condition [23]. In an earlier literature [30], we demonstrated the effect of the higher-order dispersion on the real-time dispersive Fourier transformation. The higher order dispersion induces a frequency chirp and a decrease of fringe visibility in the temporal

#115943 - $15.00 USD Received 20 Aug 2009; revised 23 Nov 2009; accepted 29 Nov 2009; published 17 Feb 2010

interferograms. In this work, since the real-time dispersive Fourier transformation is incorporated into the FMI technique for optical ranging, the theory is explained based on the instantaneous frequency concept.

The transfer function of a DCF can be expressed by expanding the mode-propagation constant β in a Taylor series [38]

$$\hat{H}(\omega) = H_a(\omega)\exp\left(-j\sum_{n=0}^{\infty}\frac{\beta_n L}{n!}\omega^n\right), \tag{1}$$

where β_n is the *nth* order mode-propagation constant, $H_a(\omega)$ is the attenuation spectrum pertaining to the loss of the DCF, ω is the angular frequency relative to the center frequency of the pulse, and L is the length of the DCF. For a femtosecond laser pulse $\hat{A}_0(\omega) = A_0(\omega)\exp[j\varphi_0(\omega)]$, where $A_0(\omega)$ is the spectral amplitude and $\varphi_0(\omega)$ is the phase distribution, the electric field of the optical pulse passing through the DCF can be expressed as

$$\hat{A}_1(\omega) = A_1(\omega)\exp[j\varphi_1(\omega)] = \hat{A}_0(\omega)\hat{H}(\omega). \tag{2}$$

Thus, the spectral phase of the pulse after passing through the DCF can be expressed as

$$\varphi_1(\omega) = \varphi_0(\omega) - \sum_{n=0}^{\infty}\frac{\beta_n L}{n!}\omega^n. \tag{3}$$

Since β_0 and β_1 have no contribution to the chromatic dispersion of the pulse, for simplicity, we define the relative group delay time as $t(\omega) = -\partial\varphi_1(\omega)/\partial\omega - t_0(\omega)$, where $t_0(\omega) = \beta_1 L$ is the average group delay. Then, $t(\omega)$ can be expressed as

$$t(\omega) = -\partial\varphi_0(\omega)/\partial\omega + \sum_{n=2}^{\infty}\frac{\beta_n L}{(n-1)!}\omega^{n-1}. \tag{4}$$

From Eq. (4), one can see that, optical slices according to different longitudinal modes of the frequency comb arrive at the photodetector with different time delay. So, after passing through a DCF, the envelope of a femtosecond optical pulse will be dispersed in the time domain. This phenomenon is used to implement an ultrafast and passive frequency sweep in this paper. The instantaneous frequency $\omega(t)$ is defined as the reciprocal of the relative group delay [26]. Considering dispersion up to β_3, with the assumption of a transform-limited pulse, i.e., $\partial\varphi_0(\omega)/\partial\omega = 0$, the instantaneous frequency can be deduced from Eq. (4) as

$$\omega(t) = \left[-1 + \sqrt{1 + X(t)}\right]\beta_2 \Big/ \beta_3, \tag{5}$$

where $X(t) = 2\beta_3 Lt/(\beta_2 L)^2$. A particular case of Eq. (5) is $\omega(0) = 0$, which means the instantaneous frequency is defined relative to the center frequency of the femtosecond pulse. The temporal FWHM of the stretched pulse is $\Delta T = DL\Delta\lambda$, where $\Delta\lambda \approx 8nm$ is the spectral FWHM of the femtosecond pulse used in this paper, and $D = -2\pi c\beta_2/\lambda^2$ is the dispersion parameter. With system parameters $\beta_2 = 98\ ps^2/km$, $\beta_3 = -0.5\ ps^3/km$ and $L \approx 12.6\,km$, the magnitude of $X(t)$ is estimated as

$$\left|X(t)\right| \approx \left|2\beta_3 L\Delta T/(\beta_2 L)^2\right| = \left|4\pi c\beta_3\Delta\lambda/\beta_2\lambda^2\right| = 0.063. \tag{6}$$

#115943 - $15.00 USD Received 20 Aug 2009; revised 23 Nov 2009; accepted 29 Nov 2009; published 17 Feb 2010

Thus, Eq. (5) can be approximated by expanding $X(t)$ in a series

$$\omega(t) = \left\{ X(t)/2 - X^2(t)/8 + O\left[X^3(t) \right] \right\} \beta_2/\beta_3 \approx c_1 t + c_2 t^2, \tag{7}$$

where, $c_1 = 1/\beta_2 L$ and $c_2 = -\beta_3 L/2(\beta_2 L)^3$. The higher order terms omitted in Eq. (7) would introduce an error less than 0.05% , which is acceptable in this work.

When the target under test is in a static state, a time delay difference τ is introduced between the object pulse and the reference pulse. And the two pulses will extend in the DCF temporally. Finally a temporal interference occurs on the photodetector with the beat frequency given by

$$\Omega(t) = \left| d\omega(t)/dt \right| \tau = c_1 \tau + 2 c_2 t \tau. \tag{8}$$

In a particular case where $\beta_3 = 0$, the temporal interferogram has a constant beat frequency $\Omega(t) = c_1 \tau$. Otherwise, $\Omega(t)$ will vary with time linearly.

In the DFMI technique, the range information is deduced from the beat frequency between the object pulse and the reference pulse. The temporal intensity $i(t)$ is proportional to the sum of the temporal intensity of each pulse and the interference term

$$i(t) \propto \left| a_1(t) \right|^2 + \left| a_1(t+\tau) \right|^2 + 2 \left| a_1(t) \right| \left| a_1(t+\tau) \right| \cos\left[\Omega(t) t \right]. \tag{9}$$

where $a_1(t)$ is the envelope of the stretched pulse, which has been analyzed in previous literatures [39,40]. If $\left| a_1(t) \right| = k \left| a_1(t+\tau) \right|$, where k is the amplitude ratio of the object pulse to the reference pulse, the intensity of the temporal interferogram can be expressed as

$$i(t) \propto i_1(t) \left\{ 1 + V_T \cos\left[\Omega(t) t \right] \right\}, \tag{10}$$

where, $i_1(t) = \left| a_1(t) \right|^2$ is the temporal intensity of the stretched pulse and $V_T = 2k/\left(1+k^2\right)$ is the visibility of the temporal interferogram.

In the frequency domain, the spectral interferogram can be expressed as

$$I(\omega) \propto I_0(\omega) \left[1 + V_S \cos(\omega \tau) \right], \tag{11}$$

where $I_0(\omega)$ is the intensity spectrum of the origin pulse and V_S is the visibility of the spectral interferogram.

By adjusting the polarization controllers, the signal intensity between two arms of the MZI could be balanced, i.e., $V_S = 1$. Then the spectral and temporal interferograms are recorded and shown in Fig. 1(b) and Fig. 1(c), respectively. Obviously, the spectral interferogram and the temporal interferogram can both be used for optical ranging. By virtue of the high repetition rate of the femtosecond laser, temporal interferograms are used for ultrafast optical ranging in [17].

2.3 Effect of the unbalanced dispersion on the DFMI

Generally, there is an unbalanced dispersion in the MZI. To analyze its effect on the DFMI, a simple mathematical model is built by adding a short length of DCF in the object arm of the MZI. Then, using Eq. (7), the instantaneous frequency of the object pulse is

$$\omega_T(t) = t/\beta_2 \left(L + \Delta L \right) - \beta_3 \left(L + \Delta L \right) t^2 \Big/ 2\left[\beta_2 \left(L + \Delta L \right) \right]^3. \tag{12}$$

The instantaneous frequency of the reference pulse is

#115943 - $15.00 USD Received 20 Aug 2009; revised 23 Nov 2009; accepted 29 Nov 2009; published 17 Feb 2010

$$\omega_R(t) = (t-\tau)/\beta_2 L - \beta_3 L(t-\tau)^2 \Big/ 2\left[\beta_2 L\right]^3. \quad (13)$$

Given a limited bandwidth of the receiver, the dispersion should be as large as possible to guarantee a large dynamic range [17]. In this work, the length of the DCF is $L \approx 12.6\,km$. Thus, condition $\Delta L/L < 10^{-5}$ is easy to be satisfied. With an assumption $\tau << \Delta T$, the beat frequency $\Omega'(t) = \left|\omega_T(t) - \omega_R(t)\right|$ can be approximated as

$$\Omega'(t) = \tau \Big/ \beta_2 L + \left[\Delta L/\beta_2 L^2 - \beta_3 \tau\left(L + 2\Delta L\right)/\left(\beta_2 L\right)^3\right] t + \beta_3 \Delta L t^2 \Big/ \left(\beta_2 L\right)^3, \quad (14)$$

where the terms containing τ^2 or ΔL^2 are omitted. According to the system parameters in this paper, with $t \approx \Delta T$ and $\tau \approx \Delta T/100$, the ratio of the last term to the first term in the right side of Eq. (14) is estimated to be 3.16×10^{-5}. Thus, Eq. (14) can be approximated as

$$\Omega'(t) \approx \tau \Big/ \beta_2 L + \left[\Delta L/\beta_2 L^2 - \beta_3 \tau L/\left(\beta_2 L\right)^3\right] t. \quad (15)$$

From Eq. (15), one can see that, even under the effects of the third order dispersion and the unbalanced dispersion, the beat frequency still varies with time almost linearly.

For general applications where the displacement range of a target is unknown, the unbalanced dispersion should be avoided. Fortunately, the unbalanced dispersion can be observed on the optical spectrum analyser directly and then be eliminated. Comparing the interference terms in Eq. (10) and Eq. (11), one can see that the temporal interferograms can be converted from the time domain into the frequency domain. Then, in order to apply the discrete Fourier transform to retrieve τ, the spectrum should be evenly sampled in the conjugate variable ω [17].

It is important to note that, Eq. (15) reveals an astonishing property of the DFMI technique. If the time delay varies very small around a given value τ_0, one can incorporate a proper length of DCF into one arm of the MZI, then the chirp rate of the beat frequency can be set to zero, i.e., $\Delta L/\beta_2 L^2 - \beta_3 \tau L/\left(\beta_2 L\right)^3 \approx 0$. In other words, the unbalanced dispersion can be used to compensate for the third order dispersion in the optical domain, within a limited dynamic range. For example, in the initialization of the system, we adjust the frequency of the interferogram to 3.5 GHz ($F_0 = \tau_0/2\pi\beta_2 L$, where $\tau_0 = 27.2\,ps$) by scanning the time delayer in the reference arm of the MZI. If the displacement of the target is within $\pm 30\mu m$, which means $\left|\Delta\tau\right| \le 0.2\,ps$. According to Eq. (15), one can incorporate a $1.416\,m$ length ($\Delta L = \beta_3 \tau_0 / \beta_2^2$) of DCF into the MZI to cancel out the frequency chirp pertaining to the third order dispersion with an accuracy that could in principle, be less than 2.3×10^{-4}.

2.4 Doppler immunity

For some dynamic applications, the conventional FMI system presented several challenges. First, the frequency deviations from a linear scanning ramp will cause a chirped beat frequency. A closed-loop control of the optical source makes the system complicated. Second, the measured results may lose reliability due to the time-consuming wavelength-scanning process. Third, it is difficult to decouple the range information and Doppler shift in the reflected object signal. But, DFMI can deal with these issues effectively. First, the wavelength scanning is performed passively based on the group velocity dispersion. The system contains neither electrical modulation devices nor mechanical moving parts. So, an effective and stable frequency-scanning ramp is guaranteed. Second, the sampling speed is on the order of tens of megahertz determined by the repetition rate of the femtosecond laser. And, the information pick-up time (exposure time) is on the order of hundreds of femtosecond determined by the

#115943 - $15.00 USD Received 20 Aug 2009; revised 23 Nov 2009; accepted 29 Nov 2009; published 17 Feb 2010

pulse duration of the laser source. During such a short period, even for an ultrafast dynamic application, one can assume that the target under test has a definite position with a constant velocity. Third, we will prove that the technique is immune to the Doppler shift.

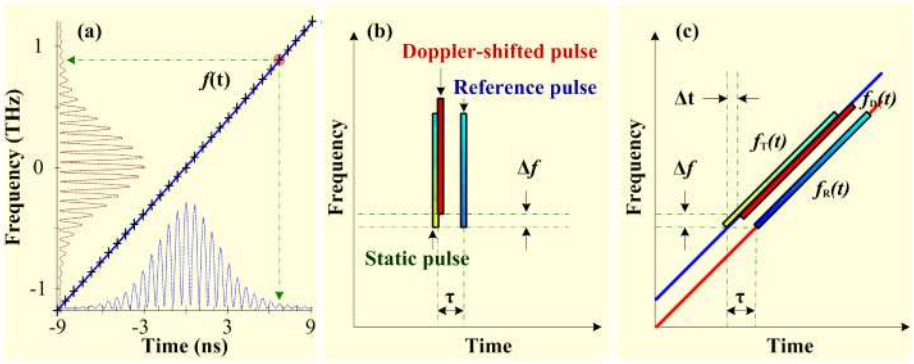

Fig. 2. Visualization of the instantaneous frequency on the frequency-time plane. (a) Time-to-frequency conversion function derived from the temporal and the spectral interferograms. (b) Femtosecond pulses before the dispersion. (c) Femtosecond pulses after the dispersion. To avoid pulse overlap, an offset perpendicular to the time-to-frequency conversion function is introduced between the Dopper-shifted pulse and the static pulse. One should also note that, generally, Doppler shift is very small relative to the optical bandwidth. For clarity, the Doppler shift is magnified in (b) and (c).

It would be explicit to explain the Doppler immunity on the time-to-frequency conversion plane. An excellent visualization of the instantaneous frequency versus relative group delay time is the Wigner-Ville distribution, which has been adopted in Ref [23]. If there is no unbalanced dispersion, a time-to-frequency conversion function is obtained using the spectral and temporal interferograms recorded on the OSA and the OSC experimentally, as shown in Fig. 2(a). From Eq. (10), (11), one can see that, a polynomial fitting function up to the second order, which relates the corresponding peak centers of the two interferograms, can be used to describe the instantaneous frequency versus the relative group delay time

$$f = \alpha_1 t + \alpha_2 t^2, \tag{16}$$

where $\alpha_1 = 1.293\times10^{20}$ and $\alpha_2 = 1.958\times10^{26}$ are the fitting coefficients. The units of frequency and time are hertz and second, respectively.

In a static state, the instantaneous frequencies of the object pulse and the reference pulse after dispersion are expressed as $f_T(t)$ and $f_R(t)$, where $f_R(t) = f_T(t-\tau)$. In a dynamic state, the Doppler frequency shift is $\Delta f = 2fv/c$, where v is the line-of-sight velocity of the target. In the dispersion process, the frequency shift Δf will introduced an extra time delay Δt on the Doppler shifted pulse relative to the static pulse, as shown in Fig. 2(b) and Fig. 2(c). Using Eq. (16), the extra delay time is $\Delta t = \Delta f / (\alpha_1 + 2\alpha_2 t)$. Then, the instantaneous frequency of the Doppler shifted pulse is

$$f_D(t) = f_T(t-\Delta t) + \Delta f, \tag{17}$$

where, $f_T(t-\Delta t)$ can be expressed using Lagrange expansion as

$$f_T(t-\Delta t) = f_T(t) + \frac{d\,f_T(t)}{dt}(-\Delta t) + \frac{d^2 f_T(t)}{2dt^2}(-\Delta t)^2 = f_T(t) - \Delta f + \alpha_2\left(\frac{\Delta f}{\alpha_2 + 2\alpha_2 t}\right)^2. \tag{18}$$

Substituting Eq. (18) into Eq. (17), the instantaneous frequency of the Doppler shifted pulse after dispersion is given by

#115943 - $15.00 USD Received 20 Aug 2009; revised 23 Nov 2009; accepted 29 Nov 2009; published 17 Feb 2010

$$f_D(t) = f_T(t) + f_E(v), \tag{19}$$

where $f_E(v) = \alpha_2 \left[2v\left(\alpha_1 t + \alpha_2 t^2\right) \Big/ c\left(\alpha_1 + 2\alpha_2 t\right) \right]^2$ is an extra frequency associated with the line-of-sight velocity of the target. So, the beat frequency is

$$\Omega''(t) = f_D(t) - f_R(t) = \left(\alpha_1 + 2\alpha_2 t\right)\tau + f_E(v). \tag{20}$$

For a given velocity $v = 100 m/s$, $f_E(v)$ is evaluated to be less than $0.01 Hz$ over the duration of the stretched pulse ($\sim 20 ns$). In the system initialization, by scanning the time delayer in the reference arm, one can turn the frequency of the generated microwave pulse to $3.5 GHz$. So, the Doppler effect is negligible; the beat frequency can be expressed as

$$\Omega''(t) = \left(\alpha_1 + 2\alpha_2 t\right)\tau. \tag{21}$$

A particular case is $\alpha_2 = 0$, then $f_E(v) = 0$. In other words, if the DCF is substituted by an optical element providing large group velocity dispersion without higher order dispersion and the dispersion in the two arms of the MZI is balanced, the system will be immune to the Doppler shift completely. A Linearly chirped fiber Bragg grating can be used to disperse the femtosecond pulse in the time domain [23], but the ripples on the linearly chirped fiber Bragg grating will degrade the range resolution. Doppler immunity has been demonstrated in Ref [35], where a $152 MHz$ Doppler shift was provided by an acousto-optic modular in the object arm of the MZI and the large velocity dispersion was provided by a linearly chirp fiber Bragg grating.

3. Experiment and data processing

In an earlier paper [30], the frequency chirp due to the third order dispersion was demonstrated. To show the effect of the unbalanced dispersion on the DFMI technique, we incorporate a 6 *m* length of DCF into the object arm and then into the reference arm of the MZI. Linear frequency chirps are observed on the optical spectrum analyser directly, as shown in Fig. 3. Obviously, the frequency chirps in Fig. 3(a) and Fig. 3(b) are opposite, due to the different location of the additional DCF inserted into the MZI.

A proof-of-concept experiment is carried out. The pulses generated by the femtosecond fiber laser have been proven to be transform-limited [30]. Dispersion compensating fibers are used to stretch the pulse in the time domain. A sinusoidal signal with a frequency of 5 *kHz* and amplitude of $5 V$ is generated by the arbitrary waveform generator and then fed to the speaker. Then the vibration of the speaker can be retrieved from the data recorded on the real-time oscilloscope using the data processing method provided in [17]. Here, a new data processing method is proposed. Since the vibrating amplitude of the speaker is less than $10 \mu m$, a $1.416 m$ length of DCF is incorporated into the reference arm to compensate for the frequency chirp due to the third order dispersion. So, the data processing can be simplified. In addition, for a dynamic implementation, the former data processing method has a poor performance, because the envelope of the interferograms may deviate from a Gaussian function occasionally, as shown in Fig. 4(a). This phenomenon may mainly due to two reasons, i.e., the pulse to pulse instability in intensity and polarization between the object signal and the reference signal. Other negative factors include the nonuniform gain spectrum of the EDFA, the nonuniform frequency response of the photodetector and the nonuniform fiber attenuation over the broad spectrum of the femtosecond laser.

#115943 - $15.00 USD Received 20 Aug 2009; revised 23 Nov 2009; accepted 29 Nov 2009; published 17 Feb 2010

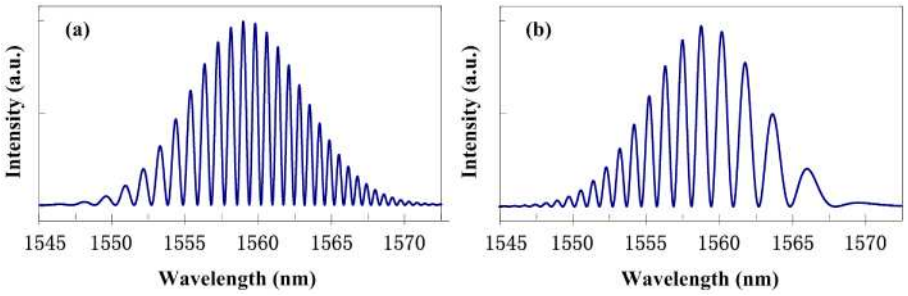

Fig. 3. Linear frequency chirp due to the unbalanced dispersion. (a) Interferogram observed on the OSA when a 6 m length DCF is incorporated in the object arm of the MZI ($\tau \approx 10 ps$). (b) Interferogram observed on the OSA when a 6 m length DCF is incorporated in the object arm of the MZI ($\tau \approx 8 ps$).

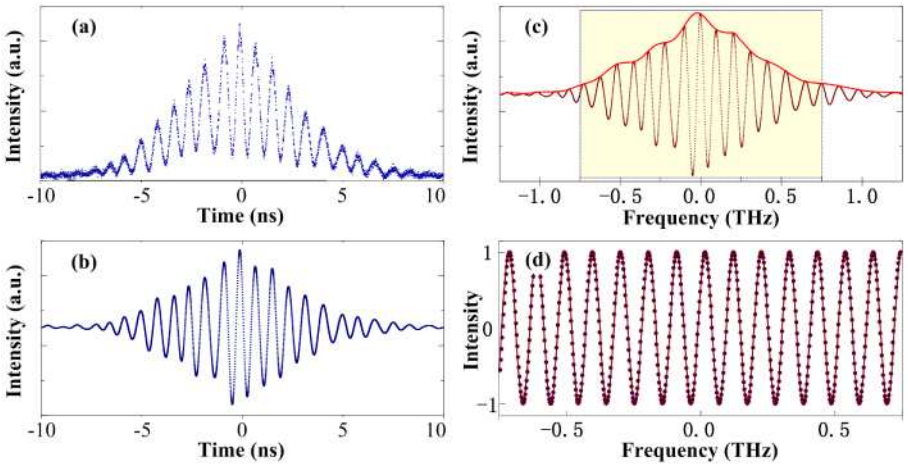

Fig. 4. (a) A typical temporal interferogram (for clarity, $\tau_0 = 9.65 ps$ is used). (b) Temporal interferogram passing through a band-pass filter. (c) Spectral interferogram transferred from the time domain. (d) Intensity normalized spectral interferogram (dots) and the sine fit result (line).

In view of these problems, we propose a general data processing method. As the first step, A FFT band-pass filtering is performed onto the raw data; thus the non-interference term in Eq. (10) and high frequency noises which may due to the cross talk of the circulator and backscattering of fiber connectors [17] are eliminated, as shown in Fig. 4(b). This operation can also be performed by adding an electrical band-pass filter between the PD and the OSC. Then the filtered waveform is transformed from the time domain into the frequency domain using $f = \alpha_1 t$, as shown in Fig. 4(c). The envelope of the spectral interferogram is obtained using the Hilbert transform. Then, the spectral interferogram can be normalized, as shown in Fig. 4(d). As the final step, τ is retrieved by applying an improved total least-squares sine fit algorithm [41] to the normalized spectrum. This non-iterative algorithm showed superior performance over traditional algorithms in accuracy, speed and convergence. In this paper, only two parameters are under estimation, i.e., the time delay difference and the phase, which further simplifies the algorithm. Considering the signal-to-noise ratio is low at the leading and trailing edges of the interferogram, only the data within an optical frequency interval of $1.5 THz$ are used to determine the sine parameters in the last step. We performed the sine fit to the data on the left side and the right side in Fig. 4(d), respectively. The final time delay difference τ is the average between the two fitting results. If τ retrieved from one side is

#115943 - $15.00 USD Received 20 Aug 2009; revised 23 Nov 2009; accepted 29 Nov 2009; published 17 Feb 2010

often larger than the value from the other side, it may indicate that the frequency chirp rate in Eq. (15) is not zero. So, one need to calibrate Eq. (16) and optimize the length of the DCF used in the MZI again. Nonlinear effects should be avoided in the experiment. Saturation of the EDFAs may also distort the normalized signal from a sine wave.

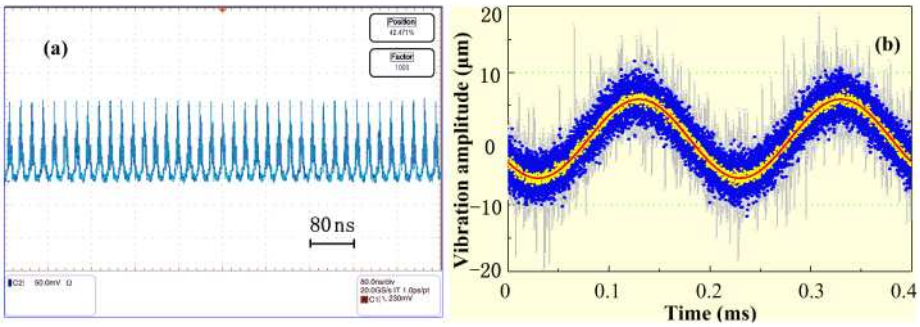

Fig. 5. (a) Picture of the temporal interferograms recorded on the OSC (Tektronix Model TDS7704B, 7 *GHz* bandwidth, 20 *Gs/s* sampling speed). (b) Vibration measurement results. Single-shot measurements based on the new data processing method (blue dots). Averaged results (yellow dots). Sine fit result (red line). Single-shot measurements based on the FFT algorithm (light gray region).

A train of the temporal interferograms recorded on the OSC is shown in Fig. 5(a), where $\tau_0 \approx 27.2\ ps$ is used. The vibration of the speaker is retrieved using the new data processing method, as shown in Fig. 5(b). A standard deviation of $1.59\ \mu m$ is estimated from the single-shot detection results with a maximum deviation of $7.59\ \mu m$. If we set the time resolution to $200\ ns$, then ten measurements can be averaged within each time bin. The averaged result is estimated to have a standard deviation of $0.49\ \mu m$, as shown in Fig. 5(b). Then, the averaged result is fitted to a sine function. The former data processing method based on the FFT and Gaussian fit algorithm is also used to retrieve the vibration from the temporal interferograms. A standard deviation of $2.43\ \mu m$ is estimated from the single-shot detection results with a maximum deviation of $21.73\ \mu m$. So, the new data processing method is better than the former one.

4. Conclusion and future research

The group velocity dispersion of a femtosecond pulse in a dispersive compensating fiber was incorporated into the frequency-modulated interferometry for ultrafast dynamic optical ranging in a dynamic experiment. The technique was immune to the Doppler shift even the higher order dispersion in the system was considered. We found that the unbalanced dispersion could be introduced in the MZI to cancel out the frequency chirp due to the third order dispersion within a limited dynamic range. The temporal interferogram and spectral interferogram were related by a constant simply. Then the time-to-frequency conversion and data re-sampling could be avoided in the simplified data processing method, which was more versatile and accurate than the previous method based on the FFT and Gaussian fit algorithms in the dynamic experiment.

It has been pointed out that, a stable mode-locked laser could provide both stable time and length metrology in space [14]. The all-fiber configuration interferometer does not require any moving optical components and can be built in a compact, robust way. Thus, it is highly suitable for space flight. For example, the technique can be used to monitor the vibration of flying wheels and detect accurate ranges between satellites. If the fiber collimator in our system is substituted by a two-dimensional spatial disperser, one can build the world's fastest camera [37]. In this work, interferometry incorporating a transform-limited femtosecond fiber

#115943 - $15.00 USD Received 20 Aug 2009; revised 23 Nov 2009; accepted 29 Nov 2009; published 17 Feb 2010

laser was adopted, making the system show great resistance to the noise in the data processing.

There are indeed some restrictions for the practical implementation of the dispersive frequency-modulated interferometry. First, for a long-term operation, the stability of the MZI is a challenge. Second, the dynamic range is restricted by the speed of the A/D converter inside the real-time oscilloscope. And the real-time storage and processing of the extremely large data is another problem. Fortunately, the range information is encoded into the frequency of the microwave pulses generated on the single-pixel photodetector. Thus, an all-optical processing of the microwave pulses rather than recording and processing the data directly, will make the dispersive frequency-modulated interferometry superior in both data processing speed and dynamic range [42].

Finally, the phase of a femtosecond pulse can be reconstructed based on the temporal interferometry [30]. An estimation of the time delay difference with a minor deviation from the true value would lead to an artificial linear chirp in the reconstructed phase. We believe that, this phenomenon can be used for optical ranging with a higher resolution.

Acknowledgements

The authors are grateful to Prof. Jianping Yao for his support in the experiments, and to the reviewers for their constructive comments. Haiyun Xia is supported by the China Scholarship Council.

#115943 - $15.00 USD Received 20 Aug 2009; revised 23 Nov 2009; accepted 29 Nov 2009; published 17 Feb 2010